

Alma Mater Studiorum Università di Bologna  
Archivio istituzionale della ricerca

Assessment of design mechanical parameters and partial safety factors for Wire-and-Arc Additive  
Manufactured stainless steel

This is the final peer-reviewed author's accepted manuscript (postprint) of the following publication:

*Published Version:*

Laghi V., Palermo M., Gasparini G., Veljkovic M., Trombetti T. (2020). Assessment of design mechanical parameters and partial safety factors for Wire-and-Arc Additive Manufactured stainless steel. ENGINEERING STRUCTURES, 225, 1-11 [10.1016/j.engstruct.2020.111314].

*Availability:*

This version is available at: <https://hdl.handle.net/11585/776741> since: 2024-03-20

*Published:*

DOI: <http://doi.org/10.1016/j.engstruct.2020.111314>

*Terms of use:*

Some rights reserved. The terms and conditions for the reuse of this version of the manuscript are specified in the publishing policy. For all terms of use and more information see the publisher's website.

This item was downloaded from IRIS Università di Bologna (<https://cris.unibo.it/>).  
When citing, please refer to the published version.

(Article begins on next page)

This is the final peer-reviewed accepted manuscript of:

Vittoria Laghi, Michele Palermo, Giada Gasparini, Milan Veljkovic, Tomaso Trombetti

## Assessment of design mechanical parameters and partial safety factors for Wire-and-Arc Additive Manufactured stainless steel

Engineering Structures, volume 225, 2020

The final published version is available online at:

<https://doi.org/10.1016/j.engstruct.2020.111314>

### Terms of use:

Some rights reserved. The terms and conditions for the reuse of this version of the manuscript are specified in the publishing policy. For all terms of use and more information see the publisher's website.

*This item was downloaded from IRIS Università di Bologna (<https://cris.unibo.it/>)*

***When citing, please refer to the published version.***

# Assessment of design mechanical parameters and partial safety factors for Wire-and-Arc Additive Manufactured stainless steel

Vittoria Laghi<sup>1\*</sup>, Michele Palermo Ph.D<sup>1</sup>, Giada Gasparini Ph.D<sup>1</sup>, Milan Veljkovic Ph.D<sup>2</sup>, Tomaso Trombetti Ph.D<sup>1</sup>

*\*corresponding author: [vittoria.laghi2@unibo.it](mailto:vittoria.laghi2@unibo.it)*

*<sup>1</sup>Department of Civil, Chemical, Environmental and Materials Engineering - University of Bologna, Viale del Risorgimento, 2 – 40136 Bologna, Italy*

*<sup>2</sup>Faculty of Civil Engineering and Geosciences- University of Technology Delft, Stevinweg, 1 – 2628CN Delft, the Netherlands*

## Abstract

Early investigations suggest that the use of Additive Manufacturing (AM) technologies for construction has the potential to decrease labor costs, reduce material waste, and create customized complex geometries that are difficult to achieve using conventional construction techniques. Nevertheless, the full exploitation of AM technologies requires data on the material mechanical properties so that reliable and safety design requirements can be developed. Among different metal-AM techniques, the so-called Wire-and-Arc Additive Manufacturing (WAAM) results to be potentially suitable to realize large-scale structural elements of any shape and size. However, the results of early experimental tests on WAAM-produced alloys suggest the need of ad-hoc considerations to properly interpret the geometrical and mechanical features of the printed outcomes. The present study analyzes the data obtained from the experimental results of tensile tests carried out on WAAM-produced 308LSi stainless steel elements with the purpose of calibrating design values and partial factors of safety. In order to take into account a possible anisotropic behavior proper of WAAM-produced elements, the design values of the main mechanical parameters have been calibrated for the three main orientations of the specimens with respect to the deposition layer. The calibrated design values and partial factors of safety for the yielding and ultimate tensile strength are compared with recommended values for stainless steel structures as found in Eurocode 3. Additional considerations upon the Young's modulus, whose values are strictly influenced by the anisotropic behavior of WAAM-produced stainless steel, are presented as well.

## Key words

Additive manufacturing; Wire-and-arc; Stainless steel structures; Calibration from experiments; Eurocode 0; Partial factors.

## 1. Introduction

Automation in construction industry has recently grown through the diffusion of digital fabrication processes which nowadays are currently employed in other industries such as aerospace and automotive [1–4]. Recent developments of Additive Manufacturing (AM) process in construction have seen the application of 3D printing techniques to realize a new generation of structures in concrete, polymers and metals [5]. In applications for steel structures, Powder-Based Fusion (PBF) technology has been adopted to realize ad-hoc connections parametrically designed either for structural optimization purposes [6] or to create free-form gridshells [7]. However, due to the intrinsic geometrical constraints of the printer environment (enclosed in a box of typically 250-mm side), the application of PBF process is limited to the realization of small-size connections and structural details [8].

In order to realize real-scale structural elements without ideally any geometrical constraints either in size or shape, the most suitable manufacturing solution for metallic elements is the so-called Wire-and-Arc Additive Manufacturing (WAAM) process. This 3D printing technology uses off-the-shelf traditional welding equipment mounted on top of either numerically-controlled robotic arms or cartesian machines, able to realize large-scale elements of several meters of dimension. The first proof-of-concept of the possibilities of the WAAM process in construction is represented by MX3D Bridge project [9], whose outcome is the first 3D-printed stainless steel footbridge completed in 2018 which will be placed in Amsterdam city center by 2020. The main advantage presented by WAAM process relies on the possibility to create new shapes and forms following the breakthrough design tools for modern architecture as algorithm-aided design with in principle no constraints either in shape or size of the printed outcome. At the same time, the WAAM process ensures fast production with good quality outcome both in terms of geometrical precision and mechanical properties. On the other hand, two additional considerations must be considered when dealing with WAAM-produced elements. First, the inherent surface roughness proper of WAAM process could influence the mechanical response. Moreover, the marked anisotropy also evidenced from the material microstructure is to take into account when defining the main mechanical parameters. Different process parameters result in different surface finishing and microstructure, both affecting the mechanical response [10].

In this regard, while several research effort has been made to study the mechanical and microstructural behavior of PBF-produced alloys [8,11–14], current research on WAAM-produced alloys focus on the microstructural analysis and provide limited information on either mechanical parameters or the anisotropic behavior of WAAM elements [15–19]. Indeed, proper mechanical

1 characterization of WAAM steel in terms of the key material properties for structural design (i.e.  
2 yielding stress, ultimate tensile strength, Young's modulus and elongation at rupture) and anisotropy  
3 is still limited to few studies [20–22]. In the work done by Gordon and co-authors [21], Young's  
4 modulus values are reported, indicating values around 130 to 140 GPa, significantly lower than the  
5 one registered by the conventional wrought material (about 190 GPa). Haden et al. [20] registered  
6 non-negligible anisotropy for WAAM stainless steel specimens in terms of ultimate tensile strength  
7 and elongation to rupture values. Kyvelou et al. [22] performed tensile tests on WAAM stainless steel  
8 specimens along three directions (longitudinal, transversal and diagonal with respect to the deposition  
9 layer), which results confirm marked anisotropy and wide range of Young's modulus values for the  
10 different orientations tested.

11 Since 2017, the authors have been studying both microstructural and mechanical characterization of  
12 WAAM-produced stainless steel elements, for structural engineering applications [23–25]. Indeed,  
13 the University of Bologna is one of the academic partner of the MX3D Bridge project (Figure 1) to  
14 characterize the 308LSi stainless steel material produced by WAAM.



16  
17 *Figure 1: The MX3D Bridge [9].*  
18

19 A first overview of the geometrical and mechanical characterization of WAAM elements for  
20 structural engineering applications is presented in [23,24]. From that, a more detailed study on the  
21 material properties of WAAM 308LSi stainless steel from the mechanical and metallurgic point of  
22 view is described in [25].

The present work analyzes the data from experimental tests with the purpose of providing a first calibration of the design mechanical properties and partial factors of safety of WAAM-produced 308LSi stainless steel elements for structural purposes.

## 2. The Wire-and-Arc Additive Manufacturing process

A basic AM system consists of a combination of a motion system, heat source and feedstock [26]. In particular, the combination of an electric arc as heat source and wire as feedstock is referred to as Wire-and-Arc Additive Manufacturing (WAAM), which currently uses standard off-the-shelf welding equipment, such as welding power source, torches and wire feeding system, while motion is provided by either robotic systems, computer numerical-controlled gantries or cartesian machines. WAAM's layer height is commonly in the range of 1 to 2 mm, resulting in an expected surface roughness of about 0.5 mm for single track deposits. As a result, this process is not considered net shape, as machining is required to finish the part, thus being better suited for low- to medium-complexity and medium- to large-scale elements, as those implemented in structural engineering [20,27–29].

The present work focuses on the particular set-up configuration of WAAM process adopted by the Dutch company MX3D [9] to realize the first 3D-printed steel footbridge.

MX3D makes use of a Gas Metal Arc Welding (GMAW) process, characterized by a continuous wire electrode which is drawn from a reel by an automatic wire feeder. The wire is fed through the contact tip in the welding torch. The heat is transferred from the welding arc and the internal resistive power causes the wire to melt [30,31].

The motion system adopted consists of industrial multi-axis ABB robots which, theoretically, are able to print from any angle. Two different printing strategies can be used: a so-called *continuous printing*, meaning that the material is deposited in continuous, and a so-called *dot-by-dot printing*, meaning that the material is deposited by successive points. The effects of these strategies on the metallurgic characteristics have been analyzed in [32,33].

Therefore, when dealing with WAAM-produced structural elements it is necessary to first codify specific issues related to: (i) the set of process parameters; (ii) the wrought material; (iii) the printing strategy. Furthermore, given the novelty of the process especially for structural engineering applications, there is very limited database of experimental results to provide sufficient information for the structural response of WAAM-produced metallic structural elements.

For such reason, the present work is limited to the study of WAAM-produced 308LSi stainless steel elements realized using continuous printing strategy. The specimens have been realized by MX3D

with a fixed set of process parameters, lying within the ranges as shown in Table 1. The welding source used is Gas Metal Arc Welding (GMAW), with pulse welding arc transfer. No arc correction has been adopted during the printing process. The substrate is a printing plate of 1000 x 1000 x 30 mm, with H-type beams welded as support. No external cooling has been used, apart from the process pauses between layers to allow the material to cool down, until it reaches a temperature below the interpass temperature of 150°.

Process parameters	Details	Value
Deposition power	Current	100 - 140 A
	Arc voltage	18 - 21 V
Speed	Welding speed	15 - 30 mm/s
	Wire feed rate	4 - 8 m/min
	Deposit rate	0.5 - 2 kg/h
Distance and angle	Layer height	0.5 - 2 mm
	Electrode to layer angle	90°
Wire	Wire grade	ER308LSi
	Wire diameter	1 mm
Shield gas	Shield gas type	98% Ar, 2%CO <sub>2</sub>
	Shield gas flow rate	10-20 L/min

*Table 1: Process parameters for WAAM deposition (Courtesy of MX3D [9]).*

When dealing with WAAM-produced structural elements, two considerations need to be further addressed: (i) the different mechanical behavior of WAAM-produced alloys with respect to the wrought material; (ii) the geometrical irregularities with respect to nominal geometrical properties. First considerations regarding those issues have been presented in [23,24].



Figure 2: Tensile specimen cut from WAAM plates: (a) as-printed and (b) after surface milling.

### 3. The experimental results

#### 3.1 Material investigation

First investigations on the material properties of WAAM-produced stainless steel material were conducted in collaboration with the Metallurgic department of University of Bologna to correlate the key material properties with the microstructural features of the printed outcomes. The results have been presented in [25].

Detailed inspection of the microstructure evidenced an oriented grain growth on the specimens. Indeed, WAAM process produced grains oriented perpendicular to the deposition layers, as presented in Figure 3. Such microstructure affects the mechanical response of specimens oriented at different directions with respect to the printing layers, as demonstrated by the tensile results presented in [22,25].

The microstructural investigations did not detect any significant defects or porosity in the specimens tested. Further details are presented in [25].

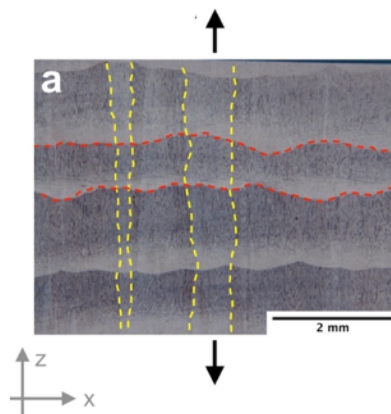




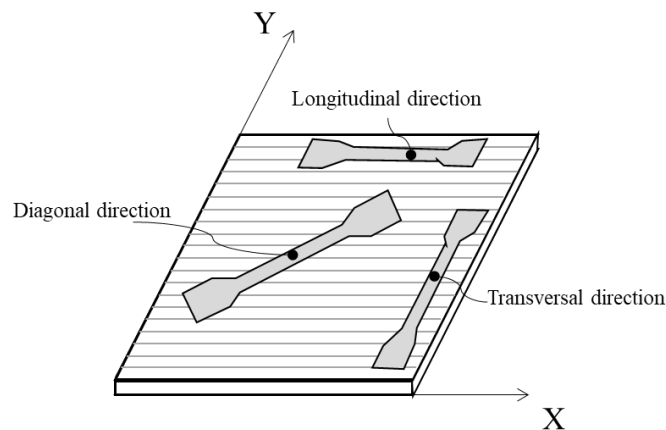
Figure 3: Microstructural grain growth (yellow) vs. deposition layer (red) for specimens oriented transversally. Black arrows indicate the loading direction (adapted from [25]).

### 3.2 Mechanical properties

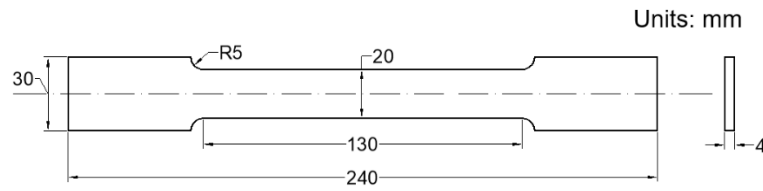
Since 2017 a wide experimental campaign has been carried out at Topography and Structural Engineering Labs at University of Bologna, in order to assess the main geometrical irregularities and mechanical properties of WAAM-produced stainless steel elements.

Experimental tests were performed on both machined and as-built specimens to evaluate the possible influence of the surface roughness, inherent in WAAM printing process, on the tensile response [24]. For the purpose of the present work, only tensile test results of machined specimens were considered. In this way, the focus is on the investigation of uncertainty on the inherent material behavior, and thus the obtained data are independent on the geometrical irregularities caused by the specific fabrication process.

The results are taken from a set of 26 tensile tests performed on samples having different orientations with respect to the deposition layer have been considered, as follows: (i) 6 tests on transversal (T) specimens oriented perpendicular to the deposition layers; (ii) 8 tests on longitudinal (L) specimens oriented along the deposition layers; (iii) 12 tests on inclined specimens oriented at  $45^\circ$ , i.e. “diagonal” (D), with respect to the deposition layers (Figure 4a). For the sake of conciseness, the three different orientations of the specimens with respect to the deposition layer will be hereafter referred to as direction L, T and D. The specimens, extracted along the three main directions as shown in Figure 4a, were shaped according to ISO 6892-1 [34] (Figure 4b). have been previously polished by means of mechanical milling, reducing the final thickness to an average value of 2.5 to 3 mm, starting from the nominal 4-mm thickness of the plates.



(a)



(b)

Figure 4: (a) Orientation of the “dog-bone” shaped specimens cut from plates with respect to the deposition layer (grey lines); (b) Geometry and dimensions (mm) of the flat tensile specimens according to ISO 6892-1 [34].

Figure 5 provides an overview of the experimental results by comparing the mean values and standard deviations of the key material properties (0.2% proof stress, ultimate tensile strength, Young’s modulus and elongation at rupture) along the three directions. Additional reference values of the key material properties for traditionally-manufactured 304L stainless steel (according to Eurocode 3 [35]) have been included as well. It should be noted that Eurocode 3 does not provide reference values for elongation at rupture of 304L stainless steel.

The results are also reported in Table 2 in terms of mean values ( $\mu_{exp}$ ), standard deviations ( $\sigma_{exp}$ ) and coefficients of variation ( $V_{exp}$ ).

		$\mu_{exp}$	$\sigma_{exp}$	$V_{exp}$
0.2% proof stress [MPa]	T	352.54	18.36	0.052
	L	338.94	20.05	0.059
	D	412.71	39.30	0.095
Ultimate tensile strength [MPa]	T	552.53	48.30	0.087
	L	567.44	17.20	0.030
	D	604.04	61.73	0.102
Young’s modulus [MPa]	T	106.09	2.98	0.028
	L	135.51	9.04	0.069
	D	244.00	34.41	0.141
Elongation at rupture [%]	T	23.47	7.27	0.310
	L	29.66	5.78	0.195
	D	22.72	5.70	0.251

Table 2: Summary of experimental results on WAAM 308LSi stainless steel.

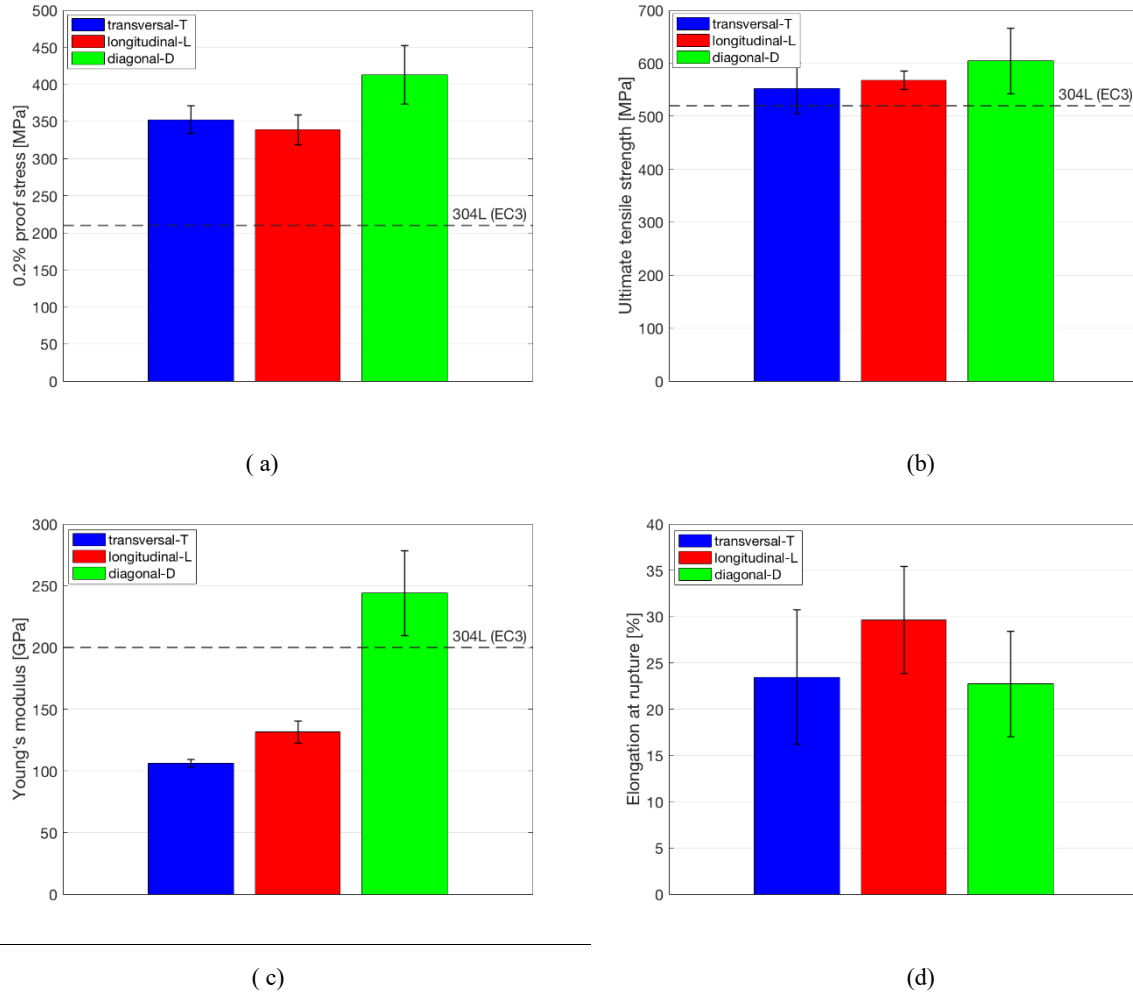


Figure 5: Overview of the experimental results: (a) 0.2% proof stress; (b) ultimate tensile strength; (c) Young's modulus; (d) elongation to rupture.

The results of the experimental campaign on WAAM 308LSi stainless steel clearly show an anisotropic behavior of the material, highly influenced by the orientation of the specimens with respect to the deposition layer (directions T, L and D). The mean values of 0.2% proof stress and ultimate tensile strength are similar for specimens oriented along T and L directions, while they increase of about 20% for 0.2% proof stress and 20% for ultimate tensile strength along D direction. Also the coefficients of variation tend to increase for specimens along D direction. The Young's modulus shows the highest sensitivity with respect to the specimens orientation. In particular, the mean value along L direction increases of about 30% with respect to that along T direction, while the mean value along D direction increases of about 120% with respect to that along T direction. Also the coefficient of variation tends to increase for specimens oriented along D direction. The values of

elongation to rupture are, on average, not significantly influenced by the orientation, even though they exhibit a quite large variability due to the influence of the microstructure on the rupture [25]. It is important to notice that Young's modulus values obtained along T and L directions are almost 40% less than the standard value of traditionally-manufactured stainless steel elements [35], while those along D direction are around 20% larger than the standard value. This anisotropic behavior is in line with the orientation of micro-grains growing perpendicular to the deposition layers (see Section 3.1), resulting in a orthotropic elastic model of WAAM material [25]. Similar results are also found in [22]. Average values of 0.2% proof stress and ultimate tensile strength do not significantly differ from those of traditionally-manufactured stainless steel. In order to properly assess the values of Young's modulus during tensile test, different measuring systems have been adopted: (i) strain gauges to locally measure the strain of the specimen during the test; (ii) deformometers for a mean measurement of the strain until first yielding occurs; (iii) optical measuring system by means of Digital Image Correlation technique to obtain information on the full field of strain during the entire test. The high variability of Young's modulus with respect to traditionally-manufactured stainless steel and its anisotropic response have been partially explained as governed by the microstructure of WAAM-produced plates [25], are still object to further research. For such reasons, the statistical interpretation and calibration of structural design values of yielding (0.2% proof) stress and ultimate tensile strength have been carried out differentiating the three main orientations of the specimens (T, L and D), including also additional considerations on the Young's modulus.

#### **4. Statistical interpretation of the experimental results**

In this section, a statistical analysis of the experimental results is carried out deriving the best fit distributions of Normal, Weibull and Log-normal according to the maximum likelihood estimators. Figure 5, 6 and 7 provide a comparison between experimental and best-fit cumulative distribution functions (CDF) and probability density functions (PDF) as obtained for yielding (0.2% proof) stress, ultimate tensile strength and Young's modulus, differentiating for the three main orientations of the specimens (T, L and D).

The dimension of the samples size, although small, is in accordance with the minimum recommended dimension according to Annex C and D of Eurocode 0 [36] to perform calibration from experiments, as long as specific values of correction factors (as reported in the provisions) are adopted. The choice of the distribution models has been made according to the indications provided in Annex C and D of

1 Eurocode 0 for strength data [36]. The mean values and standard deviations of the best-fit  
2 distributions are summarized in Table 3.

3 Overall, it should be noted that the coefficients of variation for both yielding (0.2% proof) stress and  
4 ultimate strength of all three distributions are within 2% and 10%, and in line with ranges obtained  
5 for traditionally-manufactured steel elements used in construction [37].

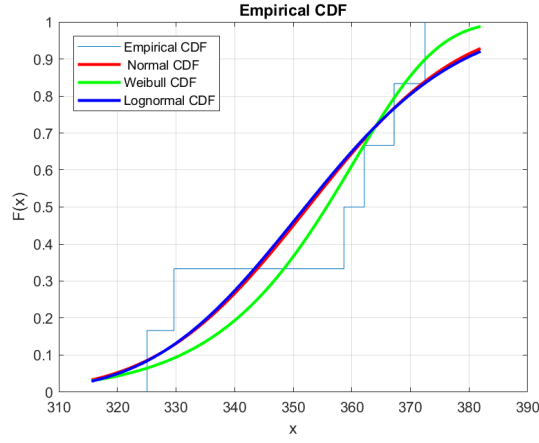
6

		NORMAL			WEIBULL			LOGNORMAL		
		$\mu_N$	$\sigma_N$	$V_N$	$\mu_W$	$\sigma_W$	$V_W$	$\mu_L$	$\sigma_L$	$V_L$
		[MPa]	[MPa]	[-]	[MPa]	[MPa]	[-]	[MPa]	[MPa]	[-]
0.2% proof stress	T	352.54	20.11	0.057	353.24	17.02	0.048	352.65	20.47	0.058
	L	338.94	21.44	0.063	338.69	21.98	0.065	339.04	21.58	0.064
	D	412.71	41.05	0.099	409.59	52.26	0.128	412.83	39.43	0.096
		$\mu_N$	$\sigma_N$	$V_N$	$\mu_W$	$\sigma_W$	$V_W$	$\mu_L$	$\sigma_L$	$V_L$
		[MPa]	[MPa]	[-]	[MPa]	[MPa]	[-]	[MPa]	[MPa]	[-]
Ultimate tensile strength	T	552.53	52.91	0.096	554.49	42.77	0.077	553.07	55.33	0.100
	L	564.22	19.73	0.035	563.64	22.22	0.039	564.25	19.64	0.035
	D	604.04	64.48	0.107	599.66	79.58	0.133	604.24	62.77	0.104
		$\mu_N$	$\sigma_N$	$V_N$	$\mu_W$	$\sigma_W$	$V_W$	$\mu_L$	$\sigma_L$	$V_L$
		[GPa]	[GPa]	[-]	[GPa]	[GPa]	[-]	[GPa]	[GPa]	[-]
Young's modulus	T	106.09	3.26	0.031	106.08	3.26	0.031	106.10	3.26	0.031
	L	131.51	9.66	0.073	130.71	12.49	0.096	131.55	9.29	0.071
	D	244.00	35.95	0.147	244.18	35.12	0.144	244.29	37.17	0.152

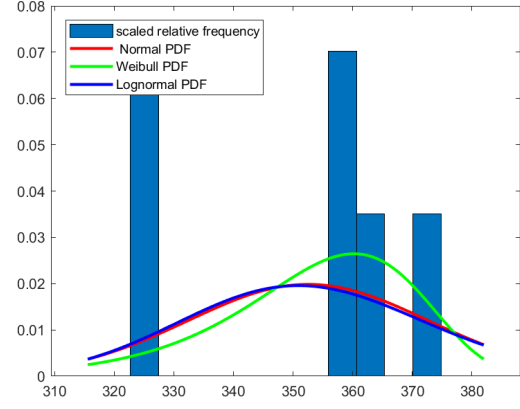
7 Table 3: Mean and standard deviation of Normal, Log-normal and Weibull best fit statistical distributions of  
8 the mechanical properties of WAAM 308LSi stainless steel.

9

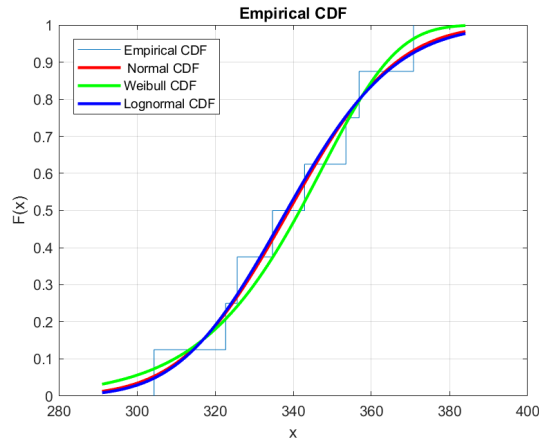
10



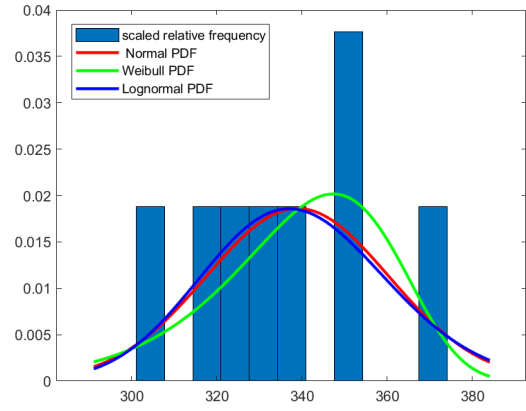
(a)



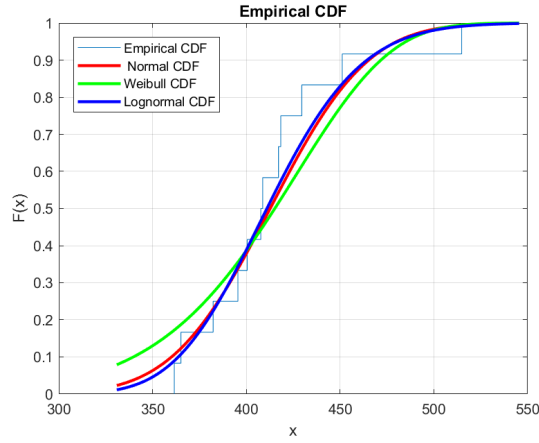
(b)



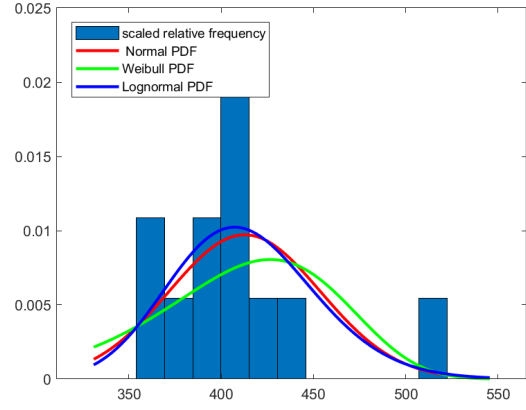
(c)



(d)

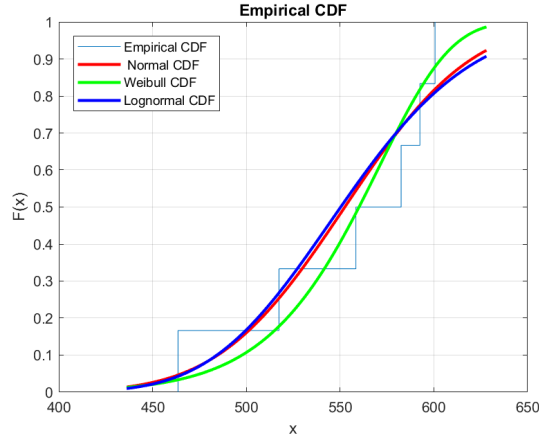


(e)

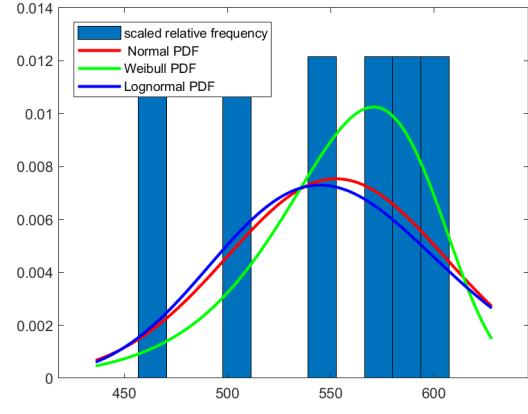


(f)

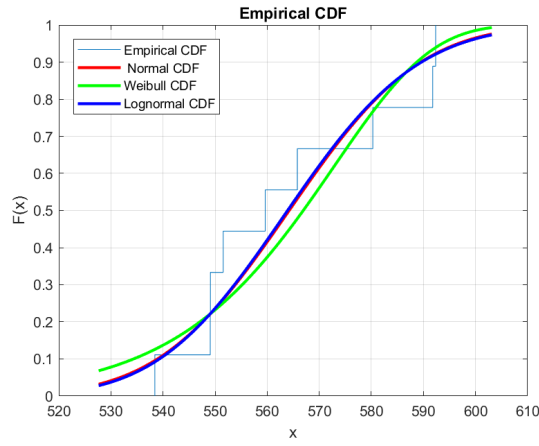
Figure 5: (a) CDF and (b) PDF of 0.2% proof stress – category T; (c) CDF and (d) PDF of 0.2% proof stress – category L; (e) CDF and (f) PDF of 0.2% proof stress – category D.



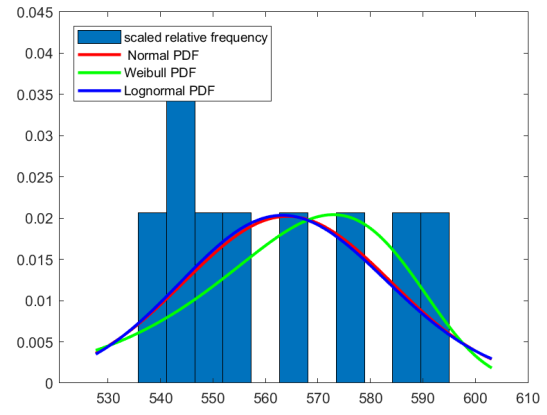
(a)



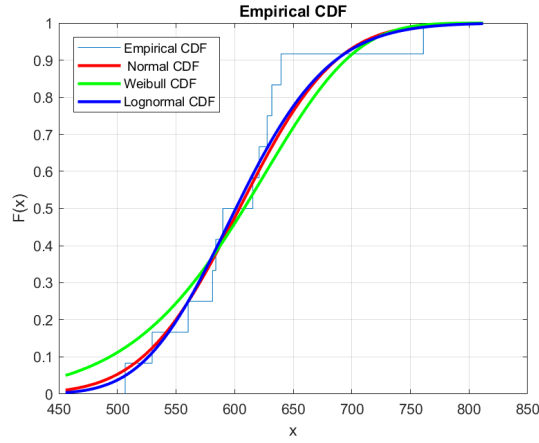
(b)



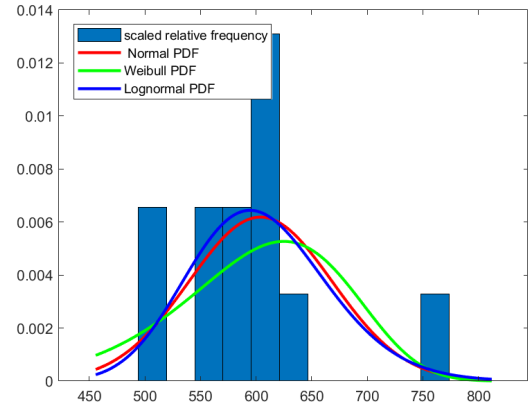
(c)



(d)

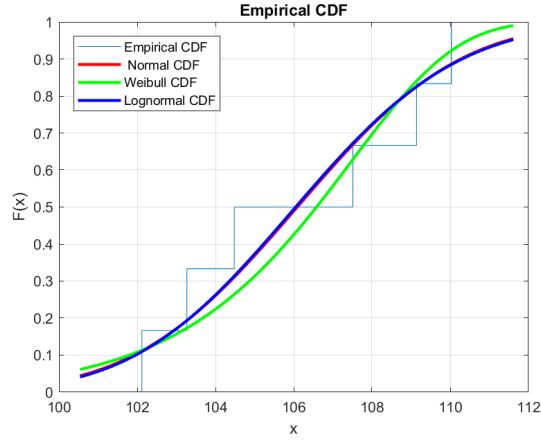


(e)

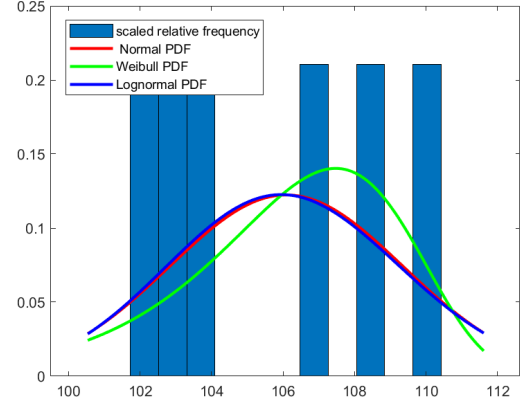


(f)

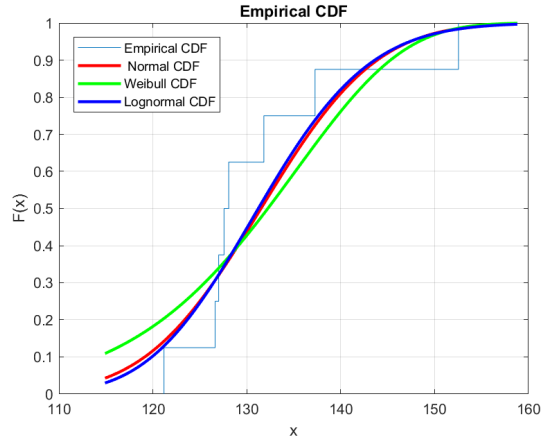
Figure 6: (a) CDF and (b) PDF of ultimate tensile strength – category T; (c) CDF and (d) PDF of ultimate tensile strength – category L; (e) CDF and (f) PDF of ultimate tensile strength – category D.



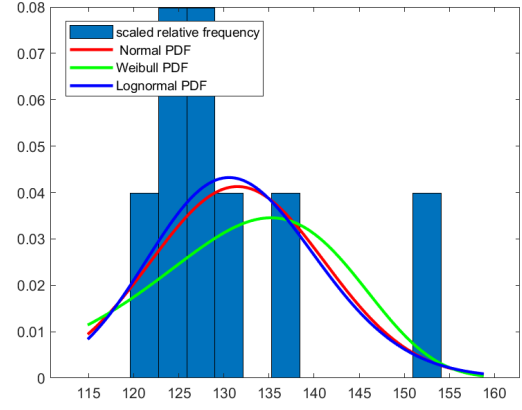
(a)



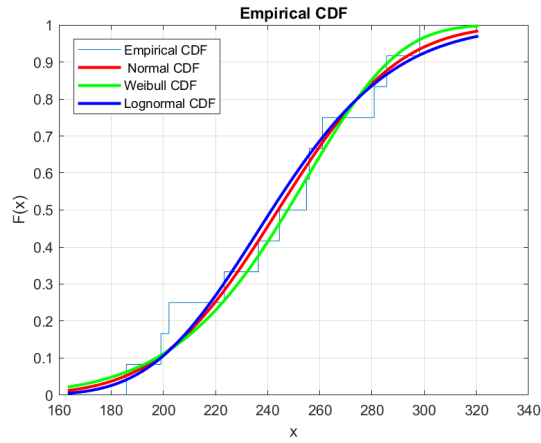
(b)



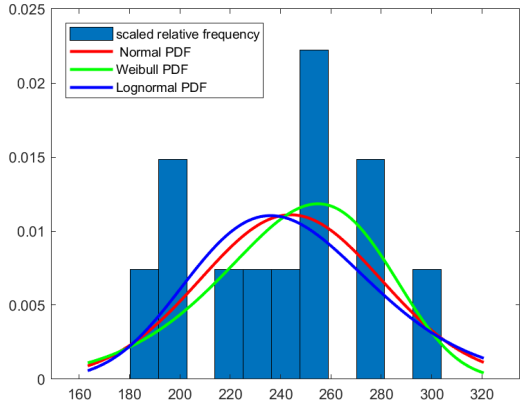
(c)



(d)



(e)



(f)

Figure 7: (a) CDF and (b) PDF of Young's modulus – category T; (c) CDF and (d) PDF of Young's modulus – category L; (e) CDF and (f) PDF of Young's modulus – category D.

Table 4 provides the results of Kolmogorov-Smirnov test in terms of coefficient KS [38] of the best-fit distributions evaluated from maximum likelihood estimators for the experimental data. The



obtained KS values range between 0.12 to 0.29. The critical values for  $\alpha=0.05$  are: 0.519 for T specimens, 0.454 for L specimens and 0.375 for D specimens.

Overall, the results provide lower values than the critical, thus suggesting that all three distributions provide a good fit with the experimental results. Among the three distributions, the Log-normal distributions provide slightly smaller values of coefficient KS (the average KS value for the Log-normal distributions is around 0.2).

Thus, in the next section the Log-normal distributions will be considered to calibrate the design values. This is also in accordance with the recommendations provided in Eurocode 0 for calibration of design values for strength.

		Kolmogorov-Smirnov test		
		KS <sub>N</sub>	KS <sub>W</sub>	KS <sub>L</sub>
		[-]	[-]	[-]
0.2% proof stress	T	0.2863	0.2432	0.2923
	L	0.1265	0.1329	0.1294
	D	0.1951	0.2248	0.1756
Ultimate tensile strength	T	0.2147	0.2265	0.2248
	L	0.1838	0.1934	0.1822
	D	0.2072	0.2512	0.1906
Young's modulus	T	0.1895	0.2360	0.1863
	L	0.2638	0.2639	0.2595
	D	0.1277	0.1285	0.1393

Table 4: Kolmogorov-Smirnov test of the Normal, Log-normal and Weibull best fit statistical distributions.

## 5. Design values of yield and ultimate stress

In this section the attention is paid to the calibration of the design values for the yielding stress ( $f_y$ ), which corresponds to 0.2% proof stress for stainless steel (according to Eurocode 3:1-4 [35]), and the ultimate tensile strength ( $f_t$ ).

The calibration of the design values of yielding and ultimate stress and corresponding partial factors is carried out considering two approaches, respectively based on the best-fit statistical distributions (Section 5.1) and on the procedure explained in Annex D of Eurocode 0 [36] (Section 5.2).

As far as the Young's modulus is concerned, for traditionally-manufactured stainless steel this quantity is commonly considered as deterministic, since its variability is negligible. However, the results of the experimental tests conducted on WAAM-produced stainless steel samples (as shown in

Section 3 and in [24,25]) revealed a significant variability in the Young's modulus values, also highly influenced by the orientation of the specimens with respect to the deposition layer. For such reason, it has been chosen to calibrate this mechanical parameter as well from statistical distributions. Considerations upon Young's modulus are presented in a dedicated section (Section 6).

### **5.1 Calibration based on the statistical distributions**

From best-fit statistical distributions as evaluated in Section 4, the fractiles corresponding to the characteristic and design values of the key material parameters have been computed. From their ratio, the estimation of the partial factor of safety is evaluated as well.

According to the fundamental principles of reliability analysis as described in EN 1990 [36], the following fractiles of the random variable associated to the strength parameters are considered:

- 5%-percentile of the distribution, corresponding to the characteristic value;
- 0.1%-percentile of the distribution, corresponding to the design value.

It should be noted that the material partial safety factor for yielding stress  $\gamma_{m1}$  is to be compared with the value of partial factor recommended in EN1993:1-4 [35] for resistance of cross-sections to excessive yielding realized in stainless steel, equal to  $\gamma_{M0}=1.10$ . Similarly, the material partial safety factor calibrated on the ultimate tensile strength  $\gamma_{m2}$  should be compared to the partial factor recommended in EN1993:1-4 [35] for resistance of cross-sections in tension to fracture realized in stainless steel, equal to  $\gamma_{M2}=1.25$ .

### **5.2 Calibration according to Eurocode 0**

European standard provisions [36] gives a simplified formulation to evaluate the characteristic value of a population of samples ("design from samples", Annex D). Considering a Log-normal distribution, the formulation is the following:

$$X_k = \exp(m_y - k_n \cdot s_y) \quad (1)$$

where  $m_y$  and  $s_y$  are respectively the estimations of mean value and standard deviation taken from the Log-normal distribution of samples, while  $k_n$  is a calibrated coefficient which takes into account the numbers of samples in the population and the type of distribution considered. For a Log-normal distribution, the values of coefficient  $k_n$  as suggested by [36] are equal to: 2.18 for specimens T (6 samples), 2.00 for specimens L (8 samples) and 1.89 for specimens D (12 samples).

Annex C of EN 1990 [36] provides also the formulation to compute the design value of the material property considered, based on the type of distribution and the probability of failure chosen for the design purposes. In the present case, the evaluations have been performed considering a probability of having a more unfavorable value of  $10^{-3}$ , typically assumed when dealing with ultimate limit states, and corresponding to a target reliability index  $\beta$  equal to 3.8.

Therefore, the design value can be evaluated with the following expression:

$$X_d = \mu_X \cdot \exp(-\alpha_R \cdot \beta \cdot V_X) \quad (2)$$

Where  $\mu_X$  and  $V_X$  are the mean and coefficient of variation of the distribution considered, and  $\alpha_R$  is the FORM sensitivity factor, usually taken equal to 0.8 for design resistances.

Thus, the partial factor for safety of the considered material property can be estimated as the ratio between the computed characteristic and design values as follows:

$$\gamma_m = \frac{X_k}{X_d} \quad (3)$$

### 5.3 Comparison of the results from calibration

Table 5 provides an overview of the results of calibration according to Eurocode 0 [36], compared with the values of fractiles as evaluated from statistical distribution of the experimental results, as from Section 4.

		5% and 0.1% fractiles from statistical distribution			Characteristic value, design value and safety factors according to EC0 [36]			EC3 recommendations for partial safety factors [35]
		$f_{y,5\%}$	$f_{y,0.1\%}$	$f_{y,5\%}/f_{y,0.1\%}$	$f_{yk}$	$f_{yd}$	$\gamma_{m1}$	
0.2% proof stress [MPa]	T	321	296	1.08	310	301	1.03	1.10
	L	305	279	1.09	297	283	1.05	
	D	353	309	1.14	343	309	1.11	
		$f_{t,5\%}$	$f_{t,0.1\%}$	$f_{t,5\%}/f_{t,0.1\%}$	$f_{tk}$	$f_{td}$	$\gamma_{m2}$	
Ultimate tensile strength [MPa]	T	469	408	1.15	443	424	1.05	1.25
	L	533	508	1.05	532	517	1.03	
	D	509	441	1.16	494	443	1.12	

Table 5: Overview of results of calibration of design values for WAAM 308LSi stainless steel.

In general, the results indicate a good correspondence between the values of 5% and 0.1% fractiles from the statistical distributions and the characteristic and design values as obtained according to Eurocode 0. In detail, the characteristic values calibrated according to Eurocode 0 are overall lower than the actual 5% fractile taken from the Log-normal distribution which best fits the experimental data. This is due to the fact that for small sample sizes, the use of large values of  $k_n$  coefficient results in a characteristic value that corresponds to a fractile smaller than the 5% one. Consequently, in this case the characteristic values get closer to the design values and therefore the corresponding partial safety factors tend to reduce. The anisotropic behavior with respect to the specimens orientation is also evidenced by the calibrated characteristic and design values and corresponding partial factors. In particular, as expected, the values of the partial factors (for both yielding and ultimate stress) along the diagonal direction tend to be larger. In any case, the values of partial safety factors suggested by Eurocode 3 [35] are in general, excluding the yielding stress along direction D, larger than those obtained in this study.

## 6. Considerations upon Young's modulus

Specific considerations on Young's modulus values are necessary to account for both the large anisotropy along the different orientations and for the intrinsic large variability of the parameter. Indeed, standard Young's modulus values of stainless steel material exhibit a quite reduced variability that is commonly neglected in the design phase.

For this aim, specific fractiles (namely 0.1%, 5%, 50%, 95% and 99.9% fractiles) have been evaluated from the best-fit statistical distributions considering the three orientations. The values reported in Table 6 clearly evidence the anisotropic behavior of Young's modulus with respect to the orientation of the specimen (T, L and D) and intrinsic variability which therefore should be taken into account during the design phase.

		Fractiles from statistical distribution				
		E <sub>0.1%</sub>	E <sub>5%</sub>	E <sub>50%</sub>	E <sub>95%</sub>	E <sub>99.9%</sub>
Young's modulus [MPa]	T	97	101	106	112	116
	L	106	117	132	148	163
	D	154	190	244	314	388

Table 6: Overview of results of distribution of Young's modulus for WAAM 308LSi stainless steel.

## 7. Conclusions

The first attempt to obtain the design values for the main mechanical properties of experimental data obtained on 308LSi stainless steel specimens fabricated by Wire-and-Arc Additive Manufacturing (WAAM) process is presented in the paper.

Indeed, the results of the experimental campaign carried out on WAAM-produced stainless steel specimens tested under tension presented a quite remarkable anisotropic behavior of the specimens based on their orientation with respect to the printing direction, namely the direction of the deposition layer. Average values of 0.2% proof stress and ultimate tensile strength are consistent with the values commonly adopted for traditionally manufactured stainless steel (e.g. 350 MPa for 0.2% proof stress and 500 MPa for ultimate tensile strength), along the three main orientations tested, i.e. along the deposition layer (longitudinal direction L), perpendicular to it (transversal direction T) and inclined 45° with respect to the deposition layer (diagonal direction D). Young's modulus values present high variability based on the orientation of the specimens: for specimens cut along directions L and T, the Young's modulus values are on average 40% less than the common value adopted for traditionally-manufactured stainless steel members (200 GPa), while for specimens along direction D the average value is 20% higher than the reference one. This anisotropic behavior is in line with the orientation of the microstructural grain growth perpendicular to the deposition layers, inducing an orthotropic elastic behavior along the two main directions (L and T), which results in higher values of elastic modulus at around 45°. Further investigations on this can be found in [25].

The preliminary calibration of the design values and partial safety factors has been carried out following two approaches, respectively based on the best-fit statistical distribution from the experiments and on the procedure explained in Annex D of Eurocode 0 [36]. For the first approach, a statistical analysis of the results of tensile tests have been performed to obtain best-fit statistical distributions of the main mechanical parameters, namely the 0.2% proof stress, ultimate tensile strength and Young's modulus.

The results from the two approaches show a good agreement between the values of the 5% and 0.1% percentiles of the statistical distributions and the corresponding characteristic and design values calibrated using the EN 1990 procedure. In particular, the characteristic values of 0.2% proof stress are between 300 and 350 MPa and the design ones between 280 and 310 MPa, varying depending on the orientation with respect to the deposition layer. The characteristic values of ultimate tensile strength are between 470 and 530 MPa and the design ones between 440 and 510 MPa, varying depending on the orientation with respect to the deposition layer. For both material properties, the

corresponding partial safety factors vary from 1.03 to 1.12. The results from both approaches are in good agreement with the values suggested for stainless steel structures as in Eurocode 3 [35]. Additional considerations have been made for the Young's modulus, for which specific fractiles (namely 0.1%, 5%, 50%, 95% and 99.9%) have been evaluated from best-fit statistical distributions considering the three main orientations of the specimens. Specific fractiles may be used depending upon different design considerations, either as lower or upper bound of the Young's modulus value. The preliminary results presented in this work are intended as a first reference for structural engineers and producers dealing with the design of structures realized with WAAM members. The long term objective is to provide contribution to deliver guidelines for the structural design of structures realized with WAAM-produced steel members.

## Acknowledgements

The support of Dutch company MX3D held in Amsterdam is gratefully acknowledged for giving the additive-manufactured specimens tested.

## Notation list

*The following symbols are used in this paper:*

$E$  = Young's modulus;

$E_{0.1\%}$  = value of Young's modulus corresponding to 0.1%-fractile from distribution;

$E_{5\%}$  = value of Young's modulus corresponding to 5%-fractile from distribution;

$E_{50\%}$  = value of Young's modulus corresponding to 50%-fractile from distribution;

$E_{95\%}$  = value of Young's modulus corresponding to 95%-fractile from distribution;

$E_{99.9\%}$  = value of Young's modulus corresponding to 99.9%-fractile from distribution;

$KS$  = Kolmogorov-Smirnov test for best-fit statistical distributions;

$V_{exp}$  = estimation of standard deviation from experiments;

$V_L$  = estimation of standard deviation for Log-normal distribution;

$V_N$  = estimation of standard deviation for Normal distribution;

$V_W$  = estimation of standard deviation for Weibull distribution;

$V_X$  = estimation of standard deviation for the random variable  $X$ ;

$X$  = random variable;

$X_d$  = design value of random variable;

$X_k$  = characteristic value of random variable;

$f_t$  = ultimate tensile strength variable;

$f_{t,0.1\%}$  = value of ultimate tensile strength corresponding to 0.1%-fractile distribution;

$f_{t,5\%}$  = value of ultimate tensile strength corresponding to 5%-fractile distribution;

$f_{td}$  = design value of ultimate tensile strength;

$f_{tk}$  = characteristic value of ultimate tensile strength;

$f_y$  = yielding stress variable;

$f_{y,0.1\%}$  = value of yielding stress corresponding to 0.1%-fractile distribution;

$f_{y,5\%}$  = value of yielding stress corresponding to 5%-fractile distribution;

$f_{yd}$  = design value of yielding stress;  
 $f_{yk}$  = characteristic value of yielding stress;  
 $k_n$  = calibration coefficient to estimate characteristic values of strength from experiments according to Annex D of EN1990 [36];  
 $m_y$  = estimation of the mean value for lognormal distributions;  
 $s_y$  = estimation of the standard deviation for lognormal distributions;  
 $\gamma_m$  = partial factor of safety related to each single material property;  
 $\gamma_{m1}$  = partial factor of safety calibrated for the yielding stress;  
 $\gamma_{m2}$  = partial factor of safety calibrated for the ultimate tensile strength;  
 $\gamma_{M0}$  = partial factor of safety for yielding (according to [36]);  
 $\gamma_{M2}$  = partial factor of safety for fracture (according to [36]);  
 $\alpha_R$  = FORM sensitivity factor;  
 $\beta$  = reliability index;  
 $\mu_{exp}$  = estimation of mean value from experiments;  
 $\mu_L$  = estimation of mean value for Log-normal distribution;  
 $\mu_L$  = estimation of mean value for Normal distribution;  
 $\mu_W$  = estimation of mean value for Weibull distribution;  
 $\sigma_{exp}$  = estimation of standard deviation from experiments;  
 $\sigma_L$  = estimation of standard deviation for Log-normal distribution;  
 $\sigma_N$  = estimation of standard deviation for Normal distribution;  
 $\sigma_W$  = estimation of standard deviation for Weibull distribution.

## References

- [1] Attaran M. The rise of 3-D printing: The advantages of additive manufacturing over traditional manufacturing. *Bus Horiz* 2017. <https://doi.org/10.1016/j.bushor.2017.05.011>.
- [2] Thomas CL, Gaffney TM, Kaza S, Lee CH. Rapid prototyping of large scale aerospace structures. 1996 IEEE Aerosp. Appl. Conf., 1998, p. 219–30.
- [3] Song Y, Yan Y, Zhang R, Xu D, Wang F. Manufacture of the die of an automobile deck part based on rapid prototyping and rapid tooling technology. *J Mater Process Technol* 2002. [https://doi.org/10.1016/S0924-0136\(01\)01165-7](https://doi.org/10.1016/S0924-0136(01)01165-7).
- [4] Giannatsis J, Dedoussis V. Additive fabrication technologies applied to medicine and health care: A review. *Int J Adv Manuf Technol* 2009;40:116–27. <https://doi.org/10.1007/s00170-007-1308-1>.
- [5] Buchanan C, Gardner L. Metal 3D printing in construction: A review of methods, research, applications, opportunities and challenges. *Eng Struct* 2019;180:332–48. <https://doi.org/10.1016/j.engstruct.2018.11.045>.
- [6] Galjaard S, Hofman S, Ren S. New Opportunities to Optimize Structural Designs in Metal by Using Additive Manufacturing. In: Block P, Knippers J, Mitra NJ, Wang W, editors. *Adv. Archit. Geom.* 2014, Cham: Springer International Publishing; 2015, p. 79–93.
- [7] Raspall F, Banon C, Tay JC. AIRTABLE. Stainless steel printing for functional space frames. *Comput Archit Des Res Asia* 2019 2019;1:113–22.
- [8] Buchanan C, Matilainen VP, Salminen A, Gardner L. Structural performance of additive manufactured metallic material and cross-sections. *J Constr Steel Res* 2017;136:35–48. <https://doi.org/10.1016/j.jcsr.2017.05.002>.
- [9] MX3D Webpage n.d. [www.mx3d.com](http://www.mx3d.com).
- [10] Dinovitzer M, Chen X, Laliberte J, Huang X, Frei H. Effect of wire and arc additive manufacturing (WAAM) process parameters on bead geometry and microstructure. *Addit Manuf* 2019;26:138–46. <https://doi.org/10.1016/j.addma.2018.12.013>.
- [11] Skiba T, Baufeld B, Van Der Biest O. Microstructure and mechanical properties of stainless steel component manufactured by shaped metal deposition. *ISIJ Int* 2009;49:1588–91.

<https://doi.org/10.2355/isijinternational.49.1588>.

- [12] Niendorf T, Leuders S, Riemer A, Richard HA, Tröster T, Schwarze D. Highly anisotropic steel processed by selective laser melting. *Metall Mater Trans B Process Metall Mater Process Sci* 2013;44:794–6. <https://doi.org/10.1007/s11663-013-9875-z>.
- [13] Guan K, Wang Z, Gao M, Li X, Zeng X. Effects of processing parameters on tensile properties of selective laser melted 304 stainless steel. *Mater Des* 2013;50:581–6. <https://doi.org/10.1016/j.matdes.2013.03.056>.
- [14] Song B, Zhao X, Li S, Han C, Wei Q, Wen S, et al. Differences in microstructure and properties between selective laser melting and traditional manufacturing for fabrication of metal parts: A review. *Front Mech Eng* 2015;10:111–25. <https://doi.org/10.1007/s11465-015-0341-2>.
- [15] Marinelli G, Martina F, Ganguly S, Williams S, Lewtas H, Hancock D, et al. Microstructure and thermal properties of unalloyed tungsten deposited by Wire + Arc Additive Manufacture. *J Nucl Mater* 2019. <https://doi.org/10.1016/j.jnucmat.2019.04.049>.
- [16] Wu W, Xue J, Wang L, Zhang Z, Hu Y, Dong C. Forming process, microstructure, and mechanical properties of thin-walled 316L stainless steel using speed-cold-welding additive manufacturing. *Metals (Basel)* 2019;9. <https://doi.org/10.3390/met9010109>.
- [17] Posch G, Chladil K, Chladil H. Material properties of CMT—metal additive manufactured duplex stainless steel blade-like geometries. *Weld World* 2017;61:873–82. <https://doi.org/10.1007/s40194-017-0474-5>.
- [18] Gu J, Wang X, Bai J, Ding J, Williams S, Zhai Y, et al. Deformation microstructures and strengthening mechanisms for the wire+arc additively manufactured Al-Mg4.5Mn alloy with inter-layer rolling. *Mater Sci Eng A* 2018;712:292–301. <https://doi.org/10.1016/j.msea.2017.11.113>.
- [19] Derekar KS. A review of wire arc additive manufacturing and advances in wire arc additive manufacturing of aluminium. *Mater Sci Technol (United Kingdom)* 2018;34:895–916. <https://doi.org/10.1080/02670836.2018.1455012>.
- [20] Haden C V., Zeng G, Carter FM, Ruhl C, Krick BA, Harlow DG. Wire and arc additive manufactured steel: Tensile and wear properties. *Addit Manuf* 2017;16:115–23. <https://doi.org/10.1016/j.addma.2017.05.010>.
- [21] Gordon J V., Haden C V., Nied HF, Vinci RP, Harlow DG. Fatigue crack growth anisotropy, texture and residual stress in austenitic steel made by wire and arc additive manufacturing. *Mater Sci Eng A* 2018;724:431–8. <https://doi.org/10.1016/j.msea.2018.03.075>.
- [22] Kyvelou P, Slack H, Mountanou DD, Wade MA, Britton T Ben, Buchanan C, et al. Mechanical and microstructural testing of wire and arc additively manufactured sheet material. *Mater Des* 2020:108675. <https://doi.org/10.1016/J.MATDES.2020.108675>.
- [23] Laghi V, Palermo M, Gasparini G, Girelli VA, Trombetti T. Geometrical characterization of Wire-and-Arc Additive Manufactured steel elements. *VBRI Press Adv Mater Lett* 2019;10:695–9.
- [24] Laghi V, Palermo M, Gasparini G, Girelli VA, Trombetti T. Experimental results for structural design of Wire-and-Arc Additive Manufactured stainless steel members. *J Constr Steel Res* 2019.
- [25] Laghi V, Palermo M, Tonelli L, Gasparini G, Ceschini L, Trombetti T. Tensile properties and microstructural features of 304L austenitic stainless steel produced by wire-and-arc additive manufacturing. *Int J Adv Manuf Technol* 2020:3693–705. <https://doi.org/10.1007/s00170-019-04868-8>.
- [26] Wong K V., Hernandez A. A Review of Additive Manufacturing. *ISRN Mech Eng* 2012;2012:1–10. <https://doi.org/10.5402/2012/208760>.
- [27] Williams SW, Martina F, Addison AC, Ding J, Pardal G, Colegrove P. Wire + Arc additive manufacturing. *Mater Sci Technol (United Kingdom)* 2016;32:641–7. <https://doi.org/10.1179/1743284715Y.0000000073>.
- [28] Uziel A. Looking at large-scale, arc-based Additive Manufacturing. *Weld J* 2016;4.
- [29] Ji L, Lu J, Liu C, Jing C, Fan H, Ma S. Microstructure and mechanical properties of 304L steel fabricated by arc additive manufacturing. *MATEC Web Conf* 2017;128. <https://doi.org/10.1051/mateconf/201712803006>.
- [30] Kim IS, Son KJ, Yang YS, Yaragada PKDV. Sensitivity analysis for process parameters in GMA welding processes using a factorial design method. *Int J Mach Tools Manuf* 2003;43:763–9. [https://doi.org/10.1016/S0890-6955\(03\)00054-3](https://doi.org/10.1016/S0890-6955(03)00054-3).



- 1 [31] Yilmaz O, Ugla AA. Microstructure characterization of SS308LSi components manufactured by  
2 GTAW-based additive manufacturing: shaped metal deposition using pulsed current arc. *Int J Adv*  
3 *Manuf Technol* 2017;89:13–25. <https://doi.org/10.1007/s00170-016-9053-y>.  
4 [32] Joosten SK. Printing a stainless steel bridge: an exploration of structural properties of stainless steel  
5 additive manufactured for civil engineering purposes. University of Technology Delft, 2015.  
6 [33] Van Bolderen GS. Exploration of stability of 3D-printed steel members. University of Technology  
7 Delft, 2017.  
8 [34] Metallic materials — Tensile testing — Part 1: Method of test at room temperature Matériaux  
9 métalliques — Essai de traction — Partie 1: Méthode d’essai à température ambiante. Iso 6892-1 2009.  
10 [35] European Committee for Standardization (CEN). EN 1993 1-4: Eurocode 3 - Design of steel structures,  
11 part 1-4: General rules, supplementary rules for stainless steel 2015.  
12 [36] European Committee for Standardization (CEN). EN 1990: Eurocode 0 - Basis of Structural Design  
13 2002.  
14 [37] Ballio G, Mazzolani FM. Strutture in acciaio. Arnoldo Mondadori Editore; 1979.  
15 [38] Jr. FJM. The Kolmogorov-Smirnov Test for Goodness of Fit. *J Am Stat Assoc* 1951;46:68–78.  
16 <https://doi.org/10.1080/01621459.1951.10500769>.  
17